A report to the sponsors of the
Exploration Geophysics Laboratory

# 2-D Modeling of Direct-S and Direct-P Wavefields
## Part 3: Reflectivity Modeling Using Real Log Data

Bob Hardage and Don Wagner

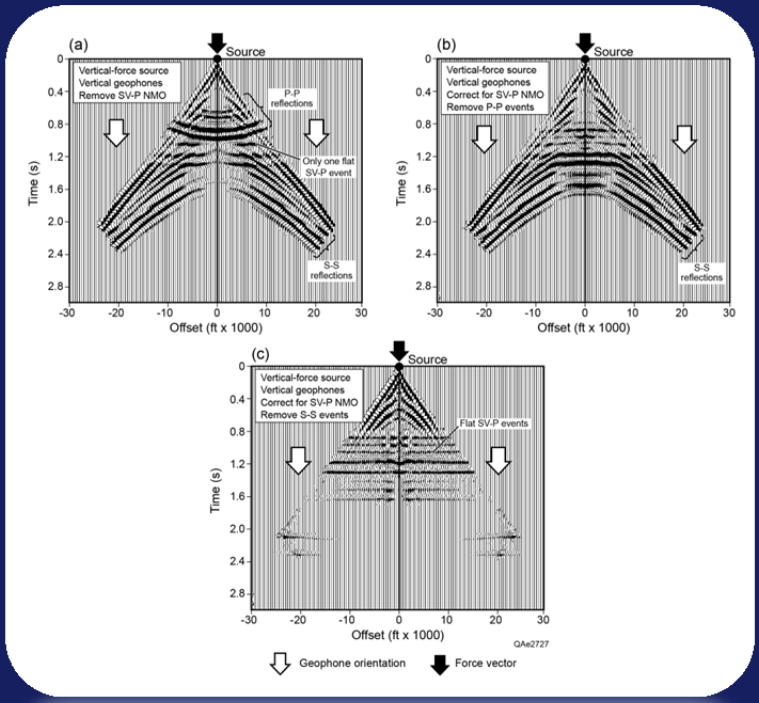


September 2014

EGL Exploration Geophysics Laboratory

Bureau of Economic Geology

QAe2977c

# 2-D Modeling of Direct-S and Direct-P Wavefields
# Part 3: Reflectivity Modeling Using Real Log Data

**Bob Hardage and Don Wagner**
**September 2014**

## Introduction

The reflectivity data calculated in this Part-3 modeling report are based on real log data. $V_P$ and $V_S$ velocity logs and their companion $\rho_b$ bulk density log are used to define the seismic propagation medium at two unconventional reservoir prospects. One study site is located in the Marcellus Shale trend in northeast Pennsylvania; the second study area is positioned at the western edge of the Midland Basin in Andrews County, Texas. Wolfberry reservoirs are the exploitation target at this second study site. These logs allow the seismic propagation medium at each location to be defined in terms of a large number of flat, horizontal, stacked thin beds. Direct-P and direct-S reflections that should be observed in surface-recorded seismic data across each prospect are calculated by applying the 2-D model code described in the preceding Part-1 and Part-2 reports of this modeling-report series (Hardage and Wagner, 2014a; 2014b) to these log-based earth models.

The calculated P and S reflections are assumed to be good approximations of real-data reflections because the log data that are utilized in the model calculations appear to be correct representations of P-wave and S-wave impedances within each seismic image space. The immediate value of the model calculations is that they provide hard evidence of the manner in which direct-P and direct-S reflections interfere with each other in surface-based data recorded by vertical and horizontal geophones. The models thus provide valuable guidance to seismic data processors who wish to extract SV-P reflections from vertical-geophone data in which there is severe interference between SV-P and P-P reflections, or when the objective is to extract S-S reflections from horizontal-geophone data when there is interference between P-SV reflections and S-S reflections.

Model results are used in this report to illustrate one procedure for extracting SV-P reflections from vertical-geophone data acquired across Marcellus and Wolfberry reservoir systems. At both prospects, the energy source used to generate the seismic data that need to be processed was a vertical-displacement source. The source at the Marcellus prospect was a shot-hole explosive, and the source at the Wolfberry prospect was an array of three inline vertical vibrators. The key model data are, therefore, direct-S and direct-P reflections generated by a vertical-displacement source. However, model data produced by a horizontal-displacement source are also calculated to illustrate how the time-offset positions of SV-P reflections produced by a horizontal-displacement source can be used to verify that SV-P reflections produced by the vertical-displacement source are properly identified.

## Marcellus Shale Model

Log data acquired at a Marcellus Shale prospect (Appalachian Basin) will be used in the first model example. The log data are displayed as Figure 1. Using these data, $V_P$, $V_S$, and ρ were defined at vertical intervals of 15-ft to create a finely sampled description of the seismic propagation medium in the vertical direction. Constant values of $V_P$ (14,837 ft/s), $V_S$ (8282 ft/s) and ρ (2.71 gm/cm$^3$) were extended from the top of the log curves to the earth surface. Thus velocity and density conditions established in the shallow layers of the earth-model are not precise representations of the near-surface conditions across this study site. Seismic receivers were distributed to large offset distances of 30,000 ft to ensure no reflections from the edges of the model would be observed during the travel time period needed to record a "seismic basement" reflection. These receivers were spaced at small horizontal intervals of 20 ft to generate a model grid that was finely sampled in the horizontal direction.

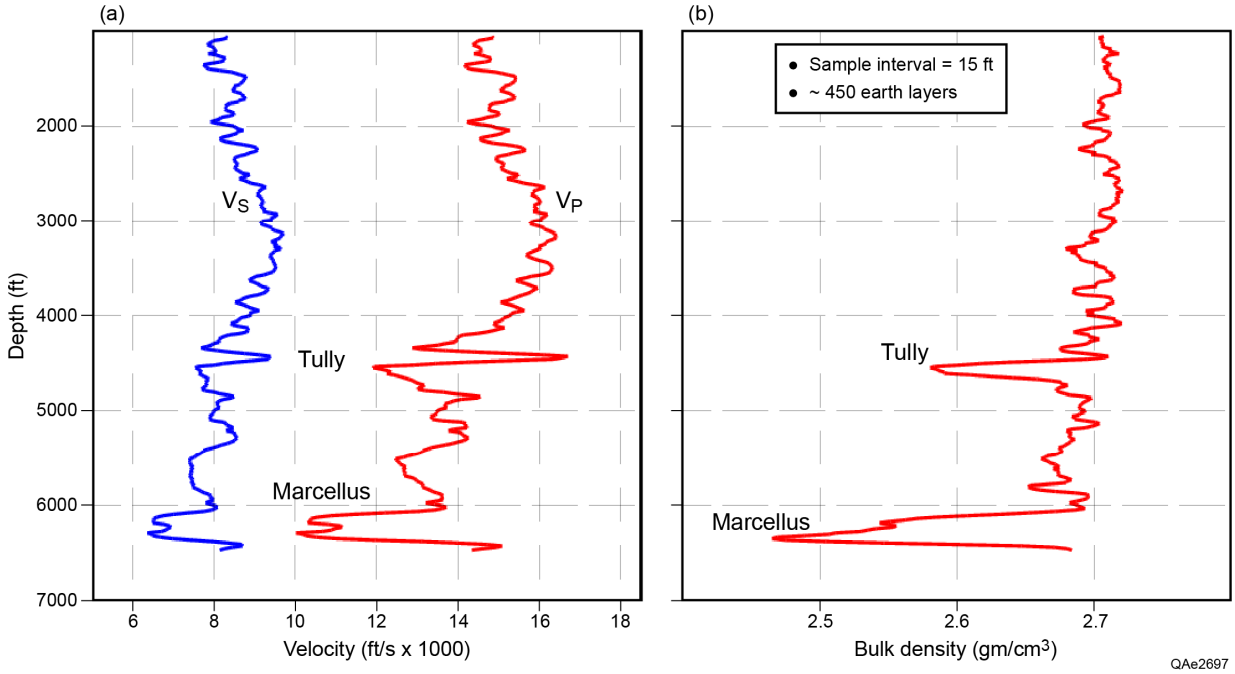


Figure 1. Log data used to create a layered earth model at an EGL Marcellus study site. Values of $V_P$, $V_S$, and ρ were defined at vertical intervals of 15 ft. (a) $V_P$ and $V_S$ data. (b) Bulk density data.

The sources used to acquire 3C3D seismic data across this site were shot-hole explosives. Thus numerical model data generated by a vertical-displacement source and recorded by both vertical and horizontal sensors would be a good approximation of the actual seismic data. However, model data were also generated by a horizontal-displacement source to aid in identifying direct-S and converted-mode reflections. Although model results can be presented as four data panels (total P, total S, X-geophone response, Z-geophone response) to illustrate the reflection physics (Hardage and Wagner, 2014a), only vertical geophone (Z) and horizontal geophone (X) responses will be shown.

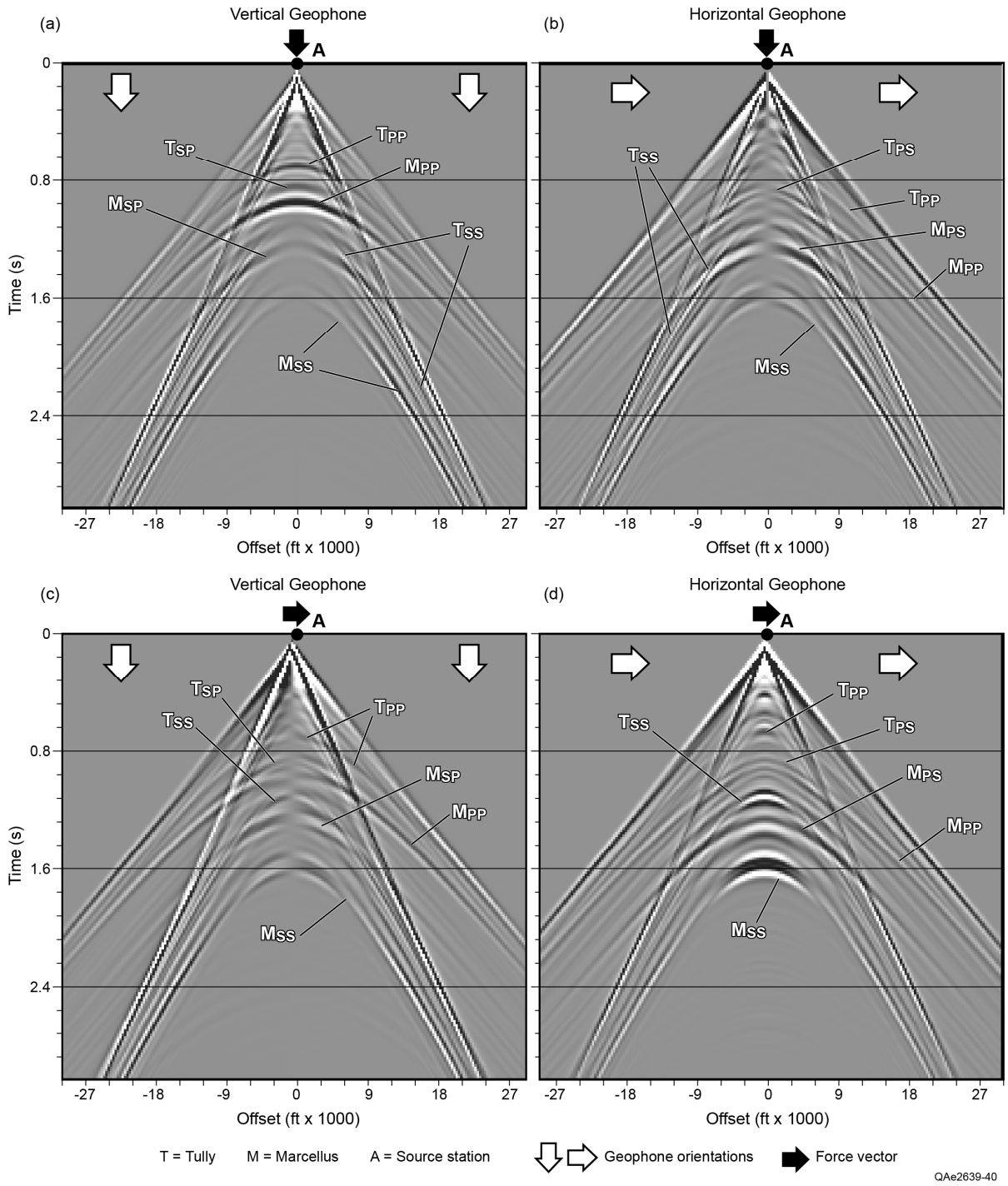


Figure 2. Model-based illumination of Marcellus Shale geology. (a) Data generated by a vertical-displacement source and recorded by vertical geophones. (b) Data generated by a vertical-displacement source and recorded by horizontal geophones. (c) Data generated by a horizontal-displacement source and recorded by vertical geophones. (b) Data generated by a horizontal-displacement source and recorded by horizontal geophones.

The data in Figure 2a show all reflections generated by a vertical-displacement source that are recorded by vertical geophones, and the data in Figure 2c show all reflections generated by a horizontal-displacement source that are recorded by the same vertical geophones. In each vertical-sensor response, some events are generated by the downgoing direct-P mode and some by the downgoing direct-S mode, whether the source is a vertical-displacement type or a horizontal-displacement type. The common factor in all events in these two data panels (Figs. 2a and 2c) is that every event is recorded by vertical sensors. Similarly, the data in Figure 2b show all reflections that are generated by a vertical-displacement source and recorded by horizontal geophones, and the data in Figure 2d show all reflections generated by a horizontal-displacement source that are recorded by the same horizontal geophones. In each horizontal-sensor response, some events are generated by the downgoing direct-P mode and some by the downgoing direct-S mode. The common factor in all events in Figures 2b and 2d is that each event is recorded by horizontal sensors.

Two geologic units dominate seismic reflection data at this Marcellus prospect – the Tully Limestone and the Marcellus Shale. The dominating impedance contrasts associated with these two geologic targets are obvious from the velocity and density behaviors labeled on the log data in Figure 1. In the synthetic wavefields exhibited in Figure 2, $T_{PP}$, $T_{PS}$, $T_{SP}$, and $T_{SS}$ are, respectively, the P-P, P-SV, SV-P, and SV-SV reflections from the Tully Limestone. $M_{PP}$, $M_{PS}$, $M_{SP}$, and $M_{SS}$ are, respectively, the P-P, P-SV, SV-P, and SV-SV reflections from the Marcellus Shale. The following principles are illustrated by these model data.

1. Data recorded by sensors oriented in the same direction as the direction in which a source applies a displacement vector have the same algebraic sign at positive-offset and negative-offset receiver stations. See Figure 2a for constant-polarity data generated by a vertical-displacement source and recorded by vertical receivers and Figure 2d for constant-polarity data generated by a horizontal-displacement source and recorded by horizontal receivers.

2. Data recorded by sensors oriented orthogonal to the direction in which a source applies a displacement vector have opposite algebraic signs at positive-offset and negative-offset receiver stations. See Figure 2b for opposite-polarity data generated by a vertical-displacement source and recorded by horizontal receivers and Figure 2c for opposite-polarity data generated by a horizontal-displacement source and recorded by vertical receivers.

3. A vertical-displacement source produces two sets of converted modes: (a) converted-P modes such as $T_{SP}$ and $M_{SP}$ (Fig. 2a), and (b) converted-S modes such as $T_{PS}$ and $M_{PS}$ (Fig. 2b). Converted-S modes are widely used by interpreters; whereas, converted-P modes are a new option for generating S attributes and S-mode images that is being promoted by EGL. Comparing Figures 2a and 2b shows $T_{SP}$ and $M_{SP}$ converted-P reflections recorded by vertical sensors occur at the same offset-travel time coordinates as do $T_{PS}$ and $M_{PS}$ converted-SV reflections recorded by horizontal sensors. The existence of these two different sets of converted modes at exactly the same positions

in vertical-geophone and horizontal-geophone gathers illustrates an important equivalence between converted-S modes and converted-P modes.

4. Robust SV-SV reflections such as $T_{SS}$ and $M_{SS}$ are created by a vertical-displacement source. These direct-S reflections are strong in horizontal-geophone gathers (Fig. 2b) and also are present, but slightly weaker, in vertical-geophone gathers (Fig. 2a). When P-P velocity analyses of vertical-geophone data are allowed to extend across a wide range of slower velocities (which is not common data-processing practice by some processors), it may be possible to recognize velocities associated with SV-P and SV-SV reflections in these slower-velocity, vertical-geophone panels in addition to seeing primary P-P reflection energies in faster-velocity panels. Likewise, P-P reflections $T_{PP}$ and $M_{PP}$ appear in horizontal-geophone data (Figs. 2c and 2d). Thus, when S-S velocity analyses of horizontal-geophone data are allowed to span a wide range of faster velocities (also not common data-processing practice by some processors), it may be possible to recognize velocities associated with P-P and P-SV reflections in these faster-velocity, horizontal-geophone panels in addition to observing SV-SV reflections observed in slower-velocity panels.

5. Primary converted-mode reflections from a shallow interface sometimes interfere with primary P-P reflections from a deep interface. An example of this undesirable outcome in this Marcellus Shale example is the interference between the shallow Tully $T_{PS}$ and $T_{SP}$ converted modes and the deep Marcellus $M_{PP}$ P-wave reflection (Figs. 2a and 2b). Inspections of Figures 2c and 2d (data produced by a horizontal-displacement source) are helpful for confirming where these reflections appear in time-offset data space in data generated by a vertical-displacement source. Similarly, SV-SV reflections from shallow interfaces may interfere with converted-mode images from a deeper interface. An example of such signal interference is shown by the shallow Tully S-wave reflection $T_{SS}$ and the deeper Marcellus converted-mode reflections $M_{PS}$ and $M_{SP}$ (Figs. 2c and 2d). This type of interference between primary reflection events associated with two different wave modes is unfortunate, but it is unavoidable in this particular geology because it is caused by the combination of the $V_P$ and $V_S$ velocities that exist in the rocks and the vertical distance between Tully and Marcellus interfaces.

These model data are invaluable for investigating data-processing strategies to isolate targeted reflections, particularly SV-P reflections. The isolation of the SV-P mode (and its companion P-SV mode) is an ideal data-processing objective because SV-P reflections are subjected to double interference (from both shallow $T_{SS}$ and deep $M_{PP}$ reflections) that causes SV-P wave-mode isolation to be challenging. The effects of applying converted-mode NMO to the source gathers of Figure 2 are presented as Figure 3.This NMO behavior was estimated from the $V_P$ and $V_S$ log-based velocities (Fig. 1). Following this NMO correction, converted-mode reflections should be approximately flat across trace-offset space. However, SV-SV reflections will be under-corrected (curved downward), and P-P reflections will be over-corrected (curved upward).

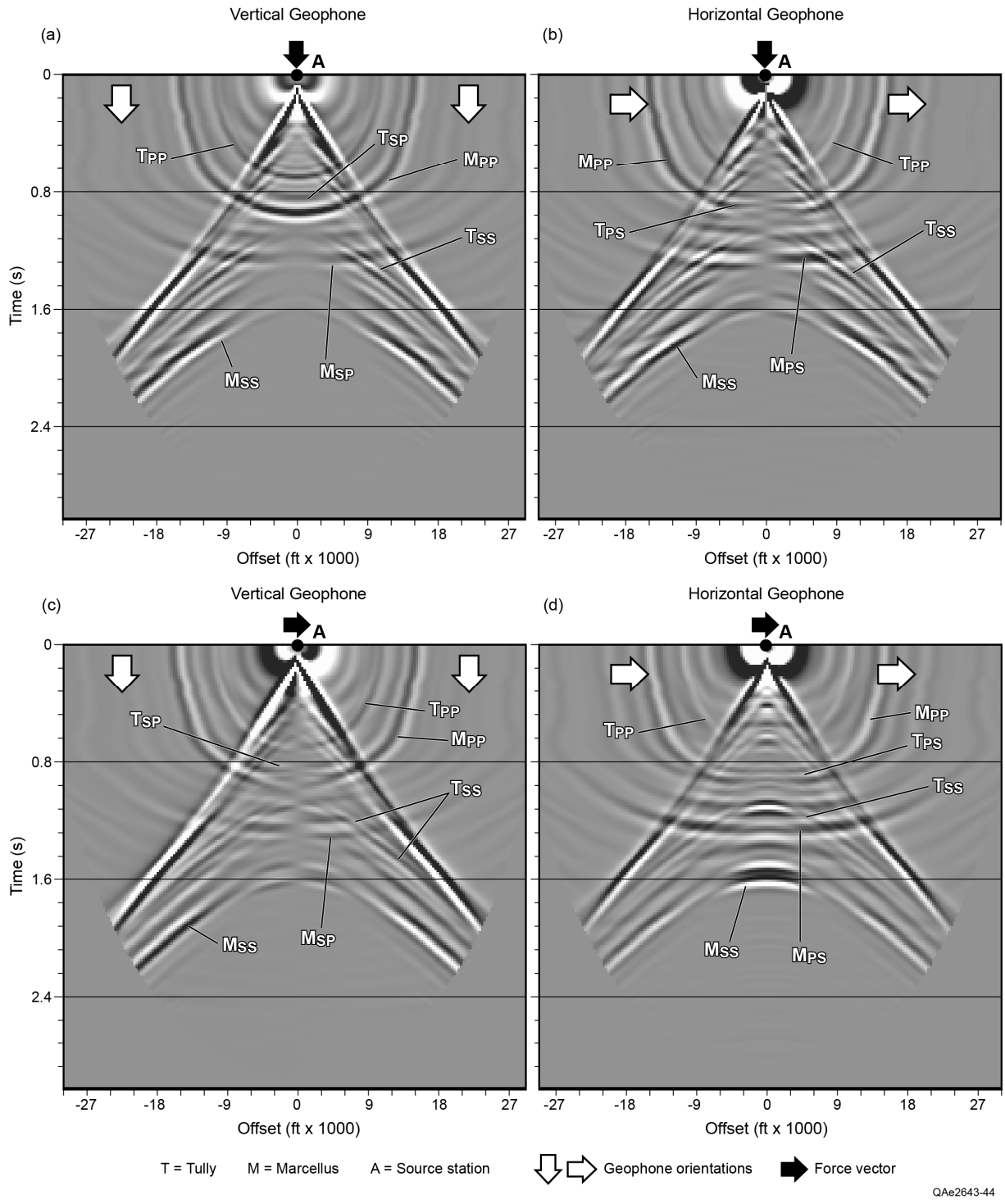


Figure 3. Application of P-SV velocity moveout to the data in Figure 2. (a) P-SV NMO applied to vertical-displacement source data recorded by vertical geophones. (b) P-SV NMO applied to vertical-displacement source data recorded by horizontal geophones. (c) P-SV NMO applied to horizontal-displacement source data recorded by vertical geophones. (d) P-SV NMO applied to horizontal-displacement source data recorded by horizontal geophones.

The NMO velocities that flatten converted-P reflections produced by a vertical-displacement source (vertical-geophone events $T_{SP}$ and $M_{SP}$ in Figure 3a) also flatten the popular converted-S modes produced the same source but recorded by horizontal geophones (events $T_{PS}$ and $M_{PS}$ in Figure 3b). This equivalence of NMO velocities for SV-P data and P-SV data is compelling evidence that these two converted modes provide identical S-wave velocity information. For the SV-P converted-P mode, the algebraic sign of positive-offset data is the same as the algebraic sign of negative negative-offset data (event $M_{SP}$ in Figure 3a). In contrast, the algebraic sign of positive-offset converted-S data is opposite to the algebraic sign of negative-offset converted-S data (event $M_{PS}$ in Figure 3b). Thus, when applying any data-processing procedure that is affected by variations in wavelet phase to data generated by a vertical-displacement source, it is essential that differences in algebraic signs caused by direction of offset from a source station be properly handled. Examples of key data-processing procedures affected by changes in wavelet polarity are velocity analyses and calculations of surface-consistent statics.

## Separating Direct-P and Direct-S Wavefields at the Marcellus Shale Prospect

This section illustrates data-processing procedures that are effective for separating converted-mode reflections when there is severe interference from P-P and SV-SV reflections. Some type of wavefield segregation strategy is particularly important for isolating the SV-P mode produced by a vertical-displacement source. Therefore, this discussion will concentrate on data-processing procedures that isolate the SV-P mode in vertical-geophone data.

In this discussion, we will not consider fast and slow modes but will assume all wavefields propagate in laterally homogeneous layering. Thus direct-P reflections will be limited to P-P and P-SV events (ignoring P-$SV_1$ and P-$SV_2$ modes). Similarly, direct-S reflections will be limited to SV-SV and SV-P events ($S_1$-$S_1$, $S_2$-$S_2$, $SV_1$-P, and $SV_2$-P modes will be ignored). In these notations, subscripts 1 and 2 indicate fast and slow modes, respectively.

In the wavefield separation strategy discussed here, the first operation is to apply SV-P NMO (identical to the P-SV NMO correction in Figure 3) to the source-gather data in Figure 2a. This NMO function is calculated from the $V_P$ and $V_S$ velocity logs shown in Figure 1. The effect of this moveout correction is illustrated in Figure 4a. After this NMO correction, SV-P reflections should be flat across the trace-gather space, but few flat events can be seen. One obvious SV-P event is labeled at approximately 1 sec. Two probable flat events follow at image times of approximately 1.2 sec and 1.3 sec, but these events are segmented by interfering SV-SV reflections.

The dominant Tully and Marcellus converted-P reflections $T_{SP}$ and $M_{SP}$ should be at approximately 0.9 and 1.2 sec, respectively. However, the data at 0.9-sec in Figure 4a are dominated by P-P reflections (upward curving events), and the 1.2-sec window is dominated by SV-SV reflections (downward curving events).These SV-SV reflections may be absent in real-world seismic data if there is a low-velocity interval immediately below the earth surface that

will bend SV raypaths to near vertical as they approach surface receiver stations. SV-SV reflections are observed in these model data because $V_P$ and $V_S$ velocities with significant magnitudes are assigned to the shallowest model layers. However, it is advantageous to have SV-SV reflections embedded in the model data because the presence of S-S reflections provides a greater data-processing challenge than does a situation where only P-P reflections interfere with SV-P reflections.

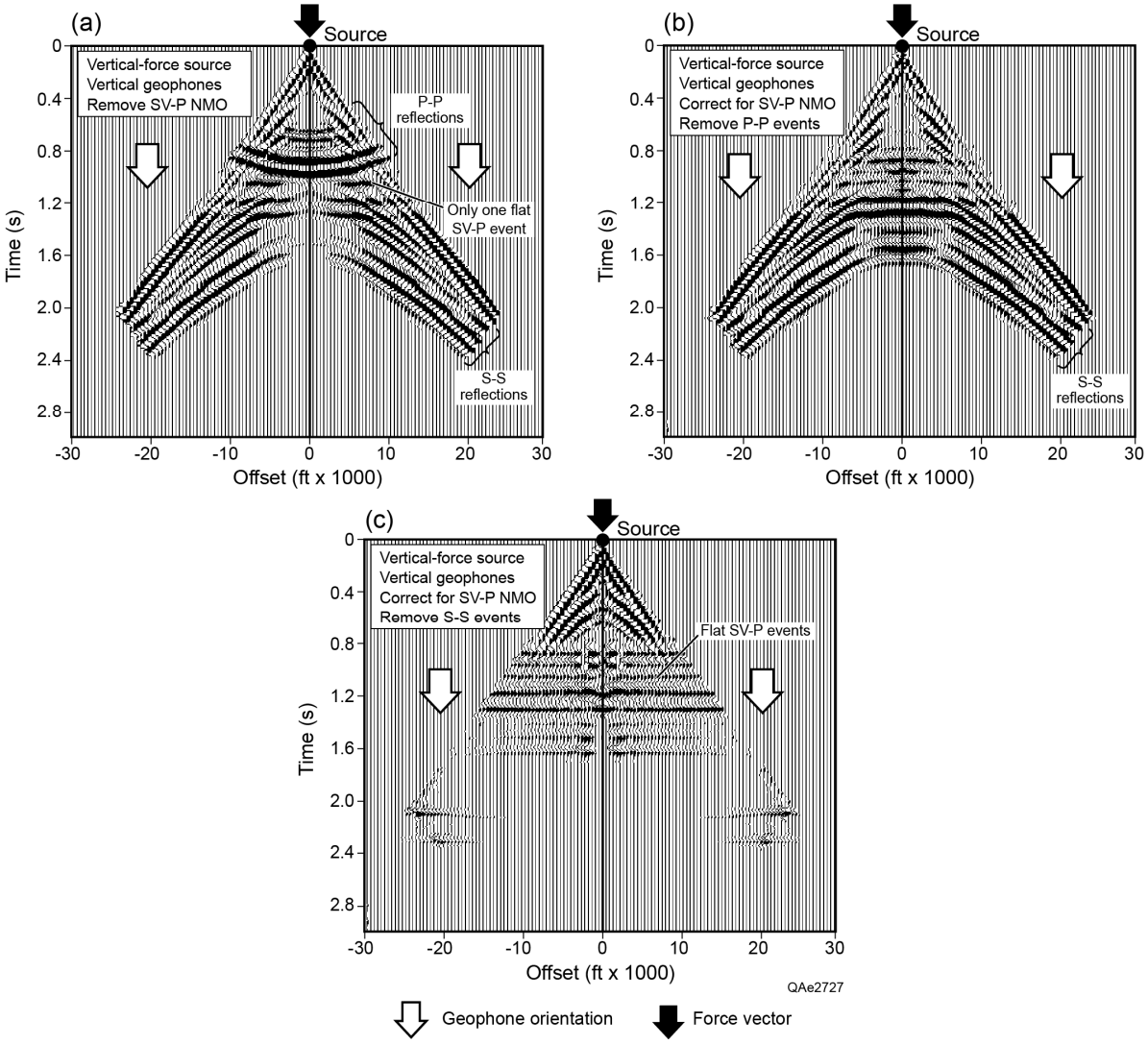


Figure 4. Isolating Marcellus SV-P modes in vertical-geophone data. (a) Vertical-displacement-source gather after SV-P NMO is applied. The flattened SV-P events are degraded by interfering P-P and SV-SV reflections. (b) Data after upward curving P-P events are attenuated. Several flat SV-P events can now be seen. (c) Data after downward curving SV-SV reflections are also attenuated. An increased number of SV-P reflections are now observed.

An algorithm that was originally designed to attenuate multiples will be used to remove the unwanted P-P and SV-SV reflections shown in Figure 4a. This algorithm can be downloaded in Fortran source code from the public Unix Seismic Processing (USP) Web site (**www.freeusp.org**). The link to the USP Web site is also provided in the reference section at the end of this report (USP, 2014). This multiple-attenuating code is named **Rmmult** in the USP software menu, and that term will be used in the following discussion. Equivalent algorithms exist in other software systems, particularly in proprietary codes used by commercial data-processing shops. Any code that allows events with targeted velocity behavior to be attenuated without imposing processor-biased, "heavy-handed" alterations of data can be used.

When **Rmmult** parameters are set so that events with curvatures similar to those of the upcurving P-P events in Figure 4a are attenuated, the result is a vertical-geophone gather with appropriately attenuated P-P reflections (Fig. 4b). The **Rmmult** process involves least-squares fits of data to specified velocity-curvature conditions to define events that are to be attenuated and least-squares adjustments to output data to remove any data anomalies that may be created. This least-squares approach not only emphasizes the flat SV-P events that are sought and suppresses P-P reflections, but it also creates minimal distortions of the residual data that remain in the trace gather. For example, the S-S reflections after **Rmmult** P-P filtering (Fig. 4b) are essentially identical to the S-S reflections before P-P filtering (Fig. 4a). A second application of the **Rmmult** algorithm was then done to attenuate downward curving SV-SV reflections. The output of this second application of **Rmmult** is shown in Figure 4c. In this latter figure, there are an increased number of good-quality SV-P reflections and a reduced number of P-P and S-S reflections.

## Wolfberry Model

The second area selected for a modeling study is a Wolfberry prospect located in the Midland Basin. The discussion figures in this section utilize the same types of model output graphics used in the preceding Marcellus Shale example. At this Wolfberry prospect, the earth model extends to a depth of approximately 11,500 ft. Earth layering was created using the log curves exhibited in Figure 5. As before, an earth layer was defined for each 15-ft increase in depth, resulting in an earth model with approximately 770 layers. Constant velocity and density values were assumed to extend from the earth surface down to the onset of measured log data. There is minimal azimuthal anisotropy and structural dip at this study site, so all earth layers are assumed to be flat, horizontal, and laterally homogeneous.

Common-source trace gathers generated from this Wolfberry model are shown in Figure 6. No reflection events are identified in terms of the stratigraphic interfaces they represent as was done for the Marcellus Shale model. There were two particularly dominating, high-energy reflections at the Marcellus site – the Tully Limestone and the Marcellus Shale – that made it easy to identify and track reflection events related to these two targets in trace gathers (Figs. 2, 3, 4). In contrast, at this Wolfberry prospect there are many reflecting interfaces, and no particular interface dominates the reflection series. As a result, more P-P

and S-S reflections interfere with SV-P reflections at this Wolfberry prospect than was the case at the Marcellus Shale site.

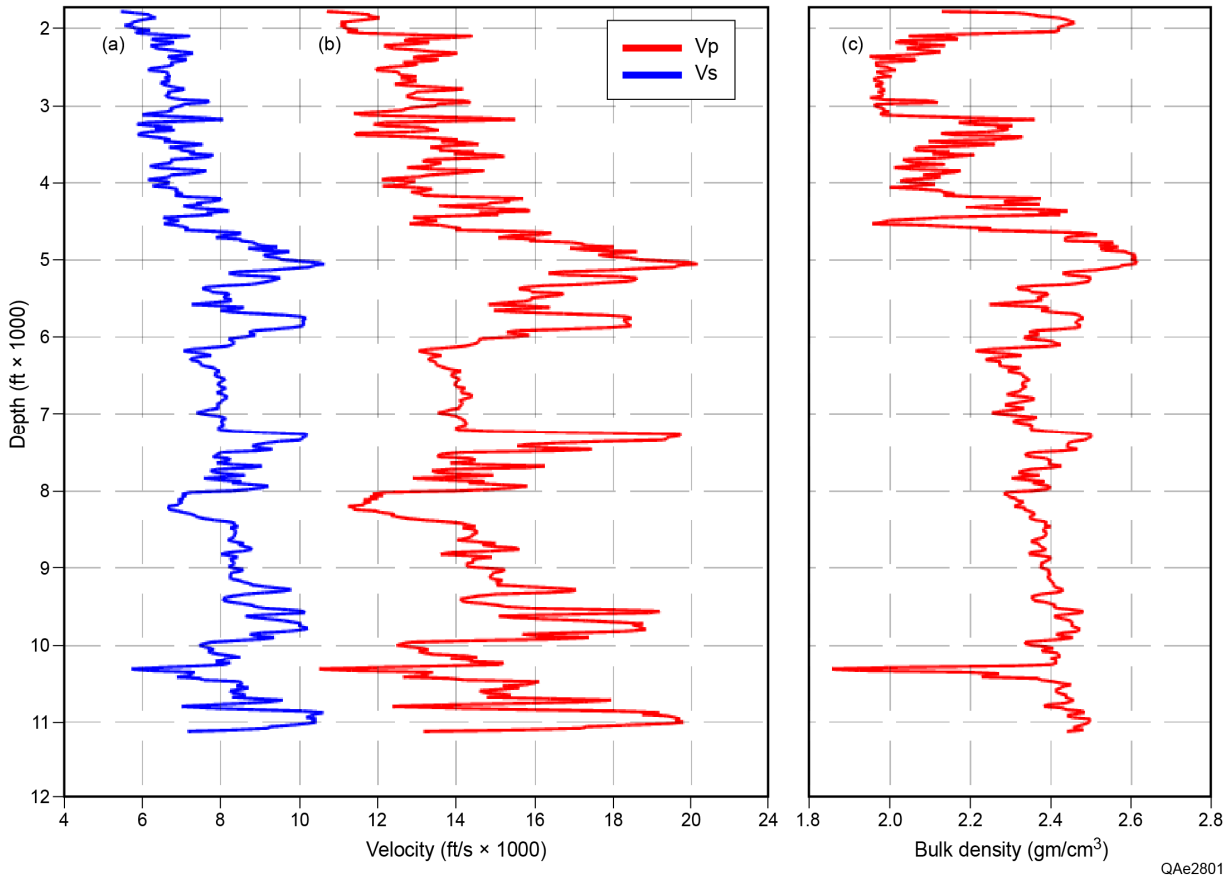


Figure 5. Log data used to create a layered earth model at an EGL Wolfberry study site. Values of $V_P$, $V_S$, and ρ were defined at vertical intervals of 15 ft. Constant velocity and density values were assumed to extend from the earth surface down to the first measured log-data values.

Figure 7 shows the results of applying SV-P NMO, offset mute, and P-P attenuation to each trace gather in Figure 6. Examination of the data panels in Figure 7 allows data processors to identify which P-P and S-S reflections are particularly troublesome as interfering events with primary SV-P reflections. Examples of wave mode interference are shown as dashed lines between time coordinates A and B labeled on Figures 7a and 7b. This insight provides a variety of ideas about how to implement data-processing strategies to attenuate targeted P-P and S-S reflections and leave relatively undisturbed SV-P reflections.

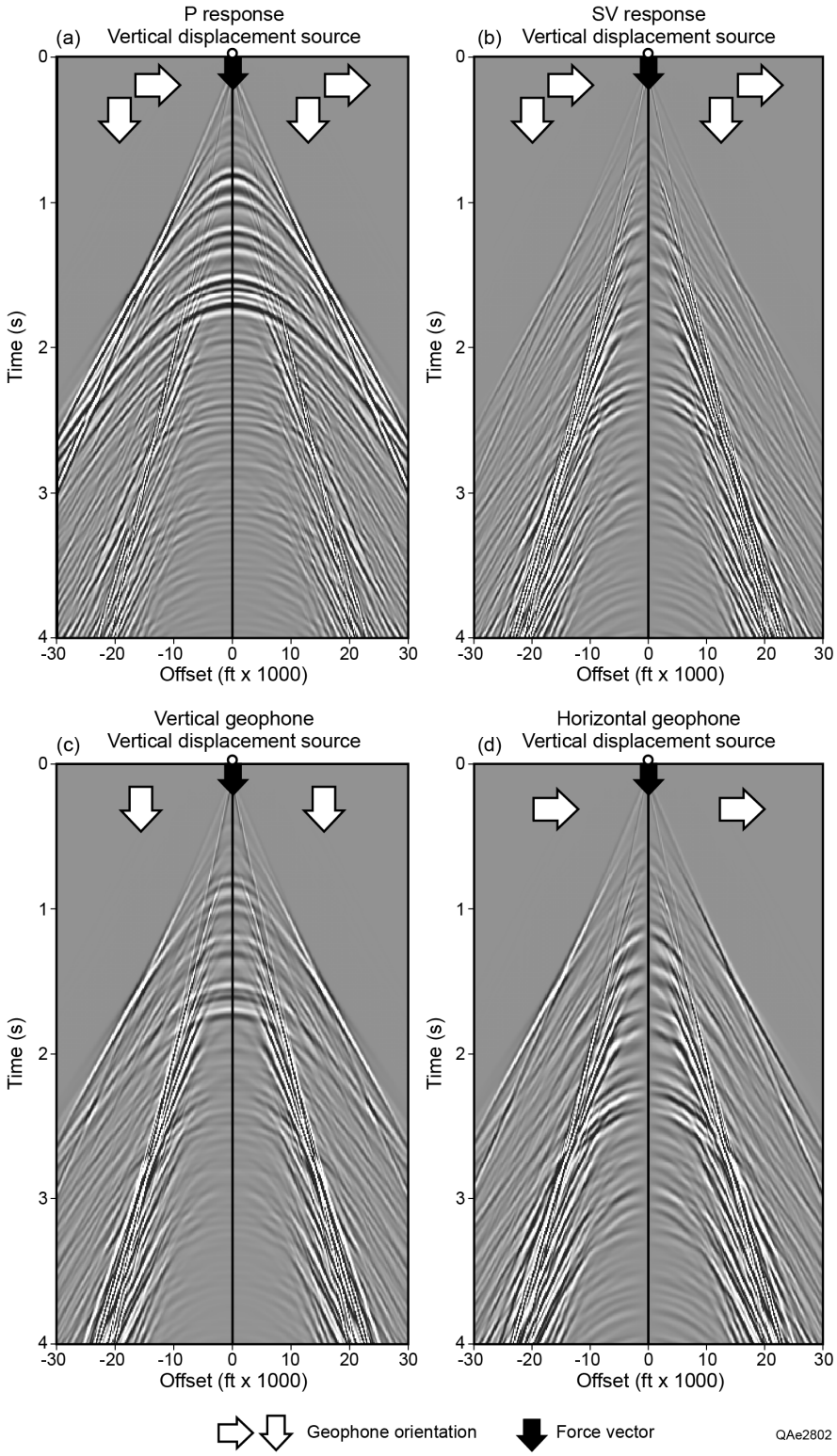


Figure 6. Illumination of Wolfberry geology. (a) P-wave data generated by a vertical-displacement source. (b) SV data generated by a vertical-displacement source. (c) Data generated by a vertical-displacement source and recorded by vertical geophones. (b) Data generated by a vertical-displacement source and recorded by horizontal geophones.

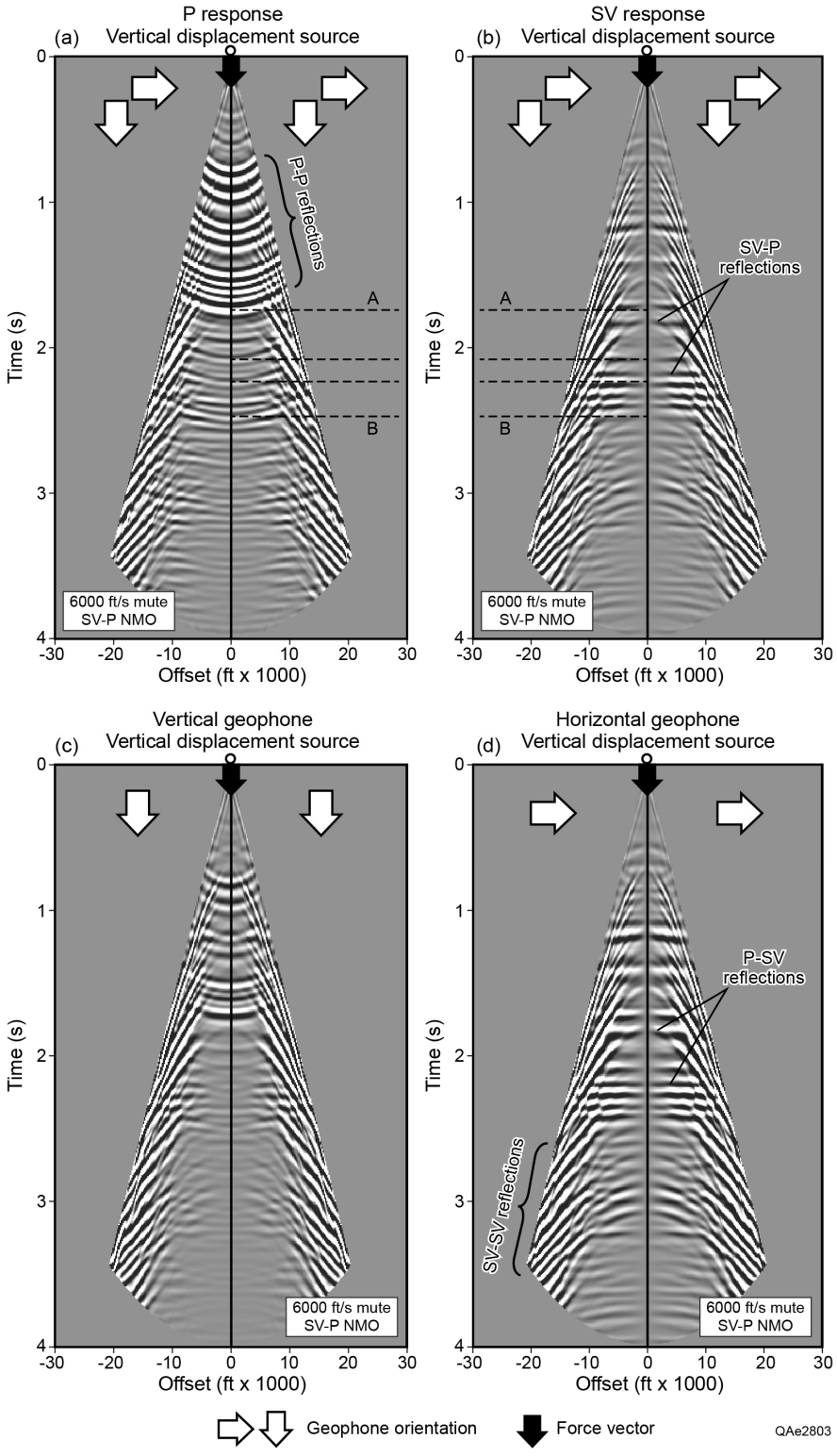


Figure 7. Application of P-SV velocity moveout, offset mute, and P-P attenuation to (a) P wavefield. (b) SV wavefield. (c) vertical-geophone data. (d) horizontal-geophone data.

The only effort made to segregate SV-P reflections from P-P and S-S reflections in the vertical-geophone data displayed in Figure 7c has been to apply an SV-P NMO correction to the vertical-geophone record. This dynamic correction flattens SV-P reflections and distinguishes SV-P events from upward curving P-P reflections and downward curving S-S reflections. However, numerous SV-P reflections are contaminated, and often totally hidden, by superimposed P-P and S-S reflections. The data in Figure 8 show the vertical-geophone record of Figure 7c after **Rmmult** is applied once to attenuate upward curving P-P events and then applied a second time to attenuate downward curving S-S reflections. The result is a rather good-quality definition of the SV-P wavefield that has minimal P-P and S-S contamination in the offset range of ±10,000 ft. Seismic data with this type of robust SV-P reflections should produce good-quality SV-P images. An application of the same mute function used in Figure 7 (6000 ft/s) would further improve the quality of the SV-P reflections in Figure 8.

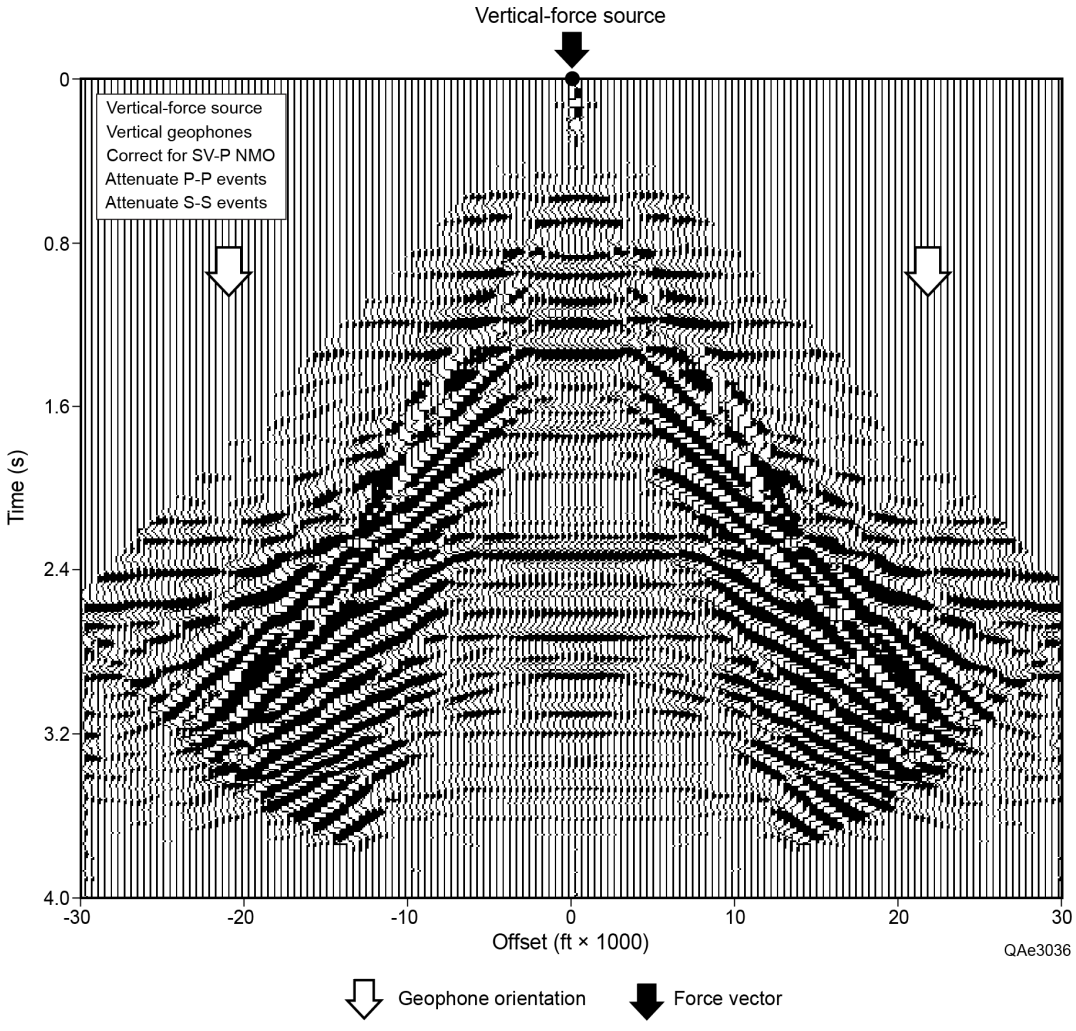


Figure 8. Unmuted version of the data in Figure 7c after three data-processing steps: (1) application of SV-P NMO, (2) attenuation of upcurving P-P reflections, and (3) attenuation of downgoing S-S reflections.

## Conclusions

This model study illustrates how the 2-D modeling code utilized at EGL can be useful to people who process direct-S data produced by vertical-displacement sources. The emphasis in this study has been on extracting the SV-P mode from vertical-geophone data because the SV-P mode appears to be the direct-S mode that will have the greatest economic impact on the geophysical profession. The earth models used in this investigation are assumed to be realistic representations of the seismic propagation medium at the two sites used in this study because the models are based on reliable log data acquired inside the 3D seismic image space at each location.

The principle message arising from this study is that data processors must devise wavefield separation methods that can be applied to vertical-geophone data because some primary SV-P reflections from shallow interfaces directly overlay primary P-P reflections from deeper interfaces. Thus P-P data are contaminated with SV-P reflections, and SV-P data are contaminated by P-P reflections. To make optimal images from either mode (P-P or SV-P), procedures need to be implemented that will separate these two interfering wavefields into one wavefield dominated by P-P reflections and a second wavefield dominated by SV-P reflections.

Such a wavefield separation can be challenging because one of the two interfering events (P-P or SV-P) will usually be weaker than the other. Thus whatever wavefield separation technique is used must be sufficiently robust to not only separate interfering P-P and SV-P events but sufficiently gentle to not alter the amplitude strength and wavelet character of either interfering reflection. This report demonstrates that one such wavefield separation technique appears to be the application of the multiple-removal algorithm **Rmmult** that can be downloaded from the public Unix Seismic Processing (USP) software library. EGL will continue to investigate other wavefield separation techniques and keep EGL sponsors apprised of our findings and conclusions.

## References

Hardage, B, and D. Wagner, 2014a, 2-D modeling of direct-S and direct-P wavefields – part 1 - modeling principles and examples: EGL Sponsor Report, private Members Area of EGL Web site.

Hardage, B, and D. Wagner, 2014b, 2-D modeling of direct-S and direct-P wavefields – part 2 - P and S radiation patterns: EGL Sponsor Report, private Members Area of EGL Web site.

USP, 2014, a compilation of valuable seismic data processing algorithm available in Fortran source code at www.freeusp.org.